AFRL-AFOSR-VA-TR-2019-0212

Hot Electron Enhanced Thermionic Emission (HEETE) Converters for All-Metal Optical Power Generation

Matthew Sheldon
TEXAS A & M UNIVERSITY

07/15/2019
Final Report

Air Force Research Laboratory
AF Office Of Scientific Research (AFOSR)/ RTB2
Arlington, Virginia 22203
Air Force Materiel Command

REPORT DOCUMENTATION PAGE

Form Approved
OMB No. 0704-0188

1. REPORT DATE *(DD-MM-YYYY)*	**2. REPORT TYPE**	**3. DATES COVERED** *(From - To)*
07-07-2019	final	April 2016 - July 2019

4. TITLE AND SUBTITLE

(YIP) Hot Electon Enhanced Thermionic Emmision (HEETE) Converters for All-Metal Optical Power Generation

5a. CONTRACT NUMBER

5b. GRANT NUMBER

FA9550-16-1-0154

5c. PROGRAM ELEMENT NUMBER

6. AUTHOR(S)

Matthew Sheldon

5d. PROJECT NUMBER

5e. TASK NUMBER

5f. WORK UNIT NUMBER

7. PERFORMING ORGANIZATION NAME(S) AND ADDRESS(ES)

TEXAS A & M UNIVERSITY
400 HARVEY MITCHELL PKY S STE 300 COLLEGE STATION TX 77845-4375
(979) 862-2841

8. PERFORMING ORGANIZATION REPORT NUMBER

9. SPONSORING/MONITORING AGENCY NAME(S) AND ADDRESS(ES)

USAF, AFRL DUNS 143574726
AF OFFICE OF SCIENTIFIC RESEARCH
875 NORTH RANDOLPH STREET, RM 3112 ARLINGTON VA 22203-1954
ELAINE UBAS 7035888391 Elaine.Ubas@us.af.mil

10. SPONSOR/MONITOR'S ACRONYM(S)

11. SPONSOR/MONITOR'S REPORT NUMBER(S)

12. DISTRIBUTION/AVAILABILITY STATEMENT

Distribution A- Approved for Public Release

13. SUPPLEMENTARY NOTES

14. ABSTRACT

This report provides a summary of major findings of our YIP supported research studying mechanisms for electron transfer that can be enhanced by photothermal energy concentration and optical excitation in plasmonic nanostructures. In particular, we have explored thermionic power conversion using nanostructured plasmonic metal absorbers that promote resonant photo-thermalization and direct photo-emission of electrons, in order to enhance the rate of electron emission.

15. SUBJECT TERMS

electron emission, plasmonics, photophysics, thermionic emission, nanophotonics, photo-thermal heating

16. SECURITY CLASSIFICATION OF:			**17. LIMITATION OF ABSTRACT**	**18. NUMBER OF PAGES**	**19a. NAME OF RESPONSIBLE PERSON**
a. REPORT	**b. ABSTRACT**	**c. THIS PAGE**			Matthew Sheldon
UU	UU	UU	UU	15	**19b. TELEPHONE NUMBER** *(Include area code)* 979-862-3101

Final Performance Report: FA9550-16-1-0154
Program Officer: Michael R. Berman
Department: Molecular Dynamics and Theoretical Chemistry

Title: Hot Electron Enhanced Thermionic Emission (HEETE) Converters for All-Metal Optical Power Generation
Primary Investigator: Matthew Sheldon, Texas A&M University

Overview: Our Young Investigator Program (YIP) supported research studied mechanisms for electron transfer that can be enhanced by photothermal energy concentration and optical excitation in plasmonic nanostructures. In particular, our research developed new strategies for thermionic power conversion using nanostructured plasmonic metal absorbers that promote resonant photothermalization and direct photo-emission of electrons, i.e. “hot” electrons, in order to enhance the rate of electron emission and power conversion efficiency. In addition, we have explored new fundamental mechanisms of inducing charge transfer in nanostructured metal geometries taking advantage of both coherent transfer of momentum directly from photons to electrons, or alternatively, geometries that have an asymmetric spatial distribution of optical absorption and photothermal heating, with relevance to emerging hot electron photochemical systems. Concurrently, we have also developed new in situ anti-stokes Raman spectroscopy techniques for quantifying both thermal and non-thermal carriers in fabricated resonant metal geometries during optical excitation, while simultaneously monitoring lattice temperature, excited electron lifetime, electron-phonon coupling, and the concomitant photo-thermal vacuum emission of hot electrons from the nanostructure surface. Taken together, our computational analysis and experiments have outlined new strategies that maximize the cooperative interactions of low energy, thermalized electrons in addition to optically excited hot carriers for photochemistry and power generation.

Major accomplishments that were achieved during the course of the grant can be organized into the following topics:

1) Optical design principles for maximizing photothermal energy concentration during optical absorption in plasmonic nanostructures.
2) A comprehensive quantum description for tunneling transport across plasmonic nanogap junctions as a strategy for optical power conversion and photochemistry.
3) Ultrafast studies of the coherent transfer of angular momentum from circularly polarized light to electrons in plasmonic Au nanoparticles, giving rise to circulating electronic currents and strong, optically induced magnetism.
4) Comprehensive analysis of photo-excited plasmonic thermionic devices in vacuum, optimized for use as optical power converters.
5) The development of new in-situ anti-stokes Raman spectroscopy techniques for quantifying the steady-state temperature and population of photo-excited hot electrons, hot electron lifetime, lattice temperature, and electron-phonon coupling in plasmonic structures.

1) Thermal Response of Plasmonic Absorbers

The optical design parameters that need to be optimized for promoting the highest possible temperature during solar absorption have been probed. Based on our photothermal analysis that accounts for the steady-state power balance between solar absorption and thermal remission of plasmonic substrates in vacuum (when conduction and convection can largely be neglected), two physical parameters dominate the photo-induced temperature response, as summarized in Figure 1. Control of the wavelength dependent absorption and emission (Figure 1 a,b,c) can be defined through surface nanostructuring such that long wavelength emission is severely constrained. In this limit, all thermal re-emission must have photon energy above the long wavelength cutoff. Thus, to maintain power balance of emission compared with the solar absorption, the device surface must reach a higher temperature, in comparison with a perfect blackbody emitter. Analogously, rather than controlling the spectral dependence of the substrate absorption and emission, it is also possible to constrain the angular range of the thermal emission (Figure 1 d,e,f). To maintain power balance with solar absorption, the surface must reach a higher temperature, so that the same power flow leaves the surface as compared with a surface that can emit with the same efficiency in every direction.

We have analyzed the temperature dependence on the specific wavelength of cutoff, the angular emission range, as well as losses associated with imperfect absorption

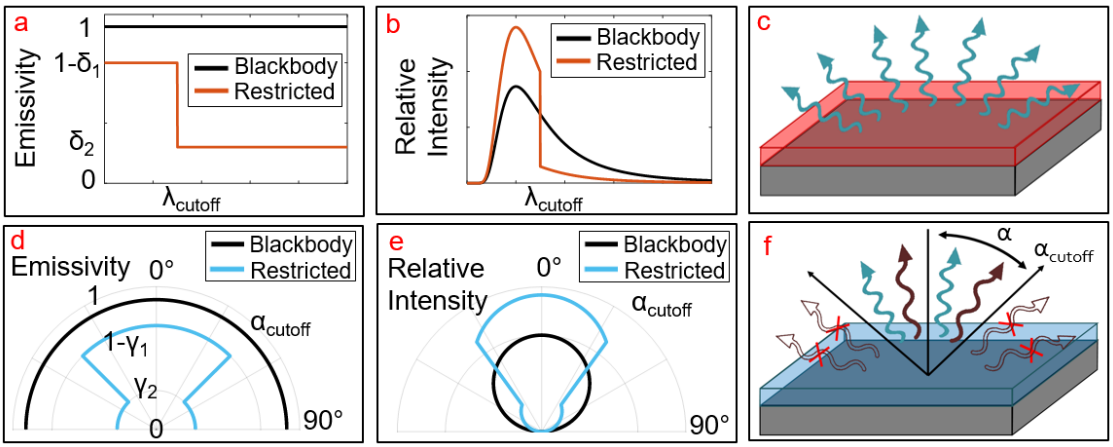

Figure 1 a) The emissivity of a wavelength-restricted surface. We model it as a step function where above some λ_{cutoff} there is an emissivity of 1- δ_1 and below the cutoff there is an emissivity of δ_2. A perfect blackbody has an emissivity of 1 across every wavelength. b) The relative intensity of the emission spectrum of a blackbody and a wavelength restricted surface during a steady-state power balance under solar illumination shows the emission in a specific wavelength range is increased for a wavelength-restricted surface, and hence the temperature must also be greater. c) Schematic of a wavelength-restricted surface. d) The emissivity of an angle restricted surface, also modeled as a step function. At small angles from normal there is an emissivity equal to 1- γ_1 while at oblique angles there is an emissivity of γ_2. A perfect blackbody has an emissivity of 1 regardless of angle. e) The relative intensity of the emission spectrum of a blackbody and angle restricted surface under solar illumination. A perfect blackbody is Lambertian and thus shows a cosine dependence of emission from a point on the surface, while an angle restricted surface shows more directional emission at higher intensity, and thus also will reach a greater temperature, since more thermal flux must leave the surface in a smaller angular range. f) Schematic of an angle restricted surface.

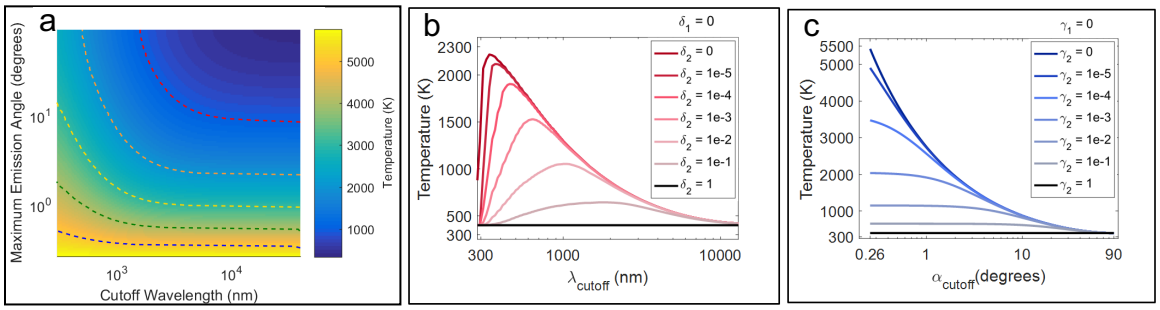

Figure 2 (a) An ideal solar absorber, with perfect absorption for wavelengths shorter than the wavelength cutoff and for angles smaller than the angular cutoff. Regardless of the wavelength response, all surfaces reach the theoretical maximum temperature corresponding to the same temperature of the sun (5800 K) when the angular range of emission is constrained to the solar disk, 0.26º (b) The thermal response of the surface when the angular emission is comparable to a smooth metal film, but there is some emission for wavelengths longer than the cutoff. The black line is the temperature response of a perfect blackbody (c) The thermal response of the surface when the wavelength response is comparable to a smooth metal film, but there is some emission outside the angular range of cutoff. Better control of the angular dependent response can provide much greater theoretical temperature increases when losses are low.

or imperfect angular, comparable with what can be anticipated in fabricated metal films. These data are summarized in Figure 2. In the limit that the plasmonic surface behaves ideally, such that the is no emission below the wavelength cutoff, or outside the angular range, and there is perfect absorption within the allowed wavelength and angular range, the performance in Figure 2a is predicted. We were surprised to learn that, independent of the frequency dependence of the absorption and emission, all surfaces will reach a theoretical maximum temperature equivalent to the temperature of the sun (5800 K), when the angular range of emission is constrained to the same angular range of the sun in the sky, or 0.26º steradians. This initial analysis therefore suggests that there is much greater benefit controlling the angular response of the metal surface, when there is a trade-off with the frequency response. In the experimental design and fabrication of our target structures, we have therefore put more emphasis into understanding and controlling the angular response.

The role of imperfect cutoff for emission is also analyzed in Figure 2 b,c. Here we find that especially when losses are comparable to what can be anticipated for fabricated metal films, in the range of 0.1-10%, the maximum possible surface temperature obtainable is more severely dependent on better control over the angular response, enabling temperature increases > 2000 K. If the angular response of the film is fixed to that of a smooth metal film, but the wavelength dependent emission is controlled with high precision, a maximum temperature of only 2300 K is possible, even with a perfect step function of the wavelength cutoff response (Figure 2b). However, if the wavelength dependent emission is comparable to a smooth film, but angular emission outside the range defined by the angle cutoff kept low, much higher temperatures can be theoretically obtained (Figure 2c). Thus, there is an intriguing possibility that plasmonically structured absorbers can out-perform state-of-the-art solar photothermal heaters, commonly called selective solar absorbers, that are currently employed in industry for solar water heating and other applications that scavenge solar-thermal energy. Current materials only control for the wavelength dependence of absorption and emission, without the level of control over the angular dependence that can be achieved by nanostructuring metal thin films.

Moreover, the strategy we are pursuing does seem to allow significant enough temperatures, greater than 900 K even with realistic losses, that will allow appreciable efficiencies for HEETE power conversion during non-concentrated solar illumination.

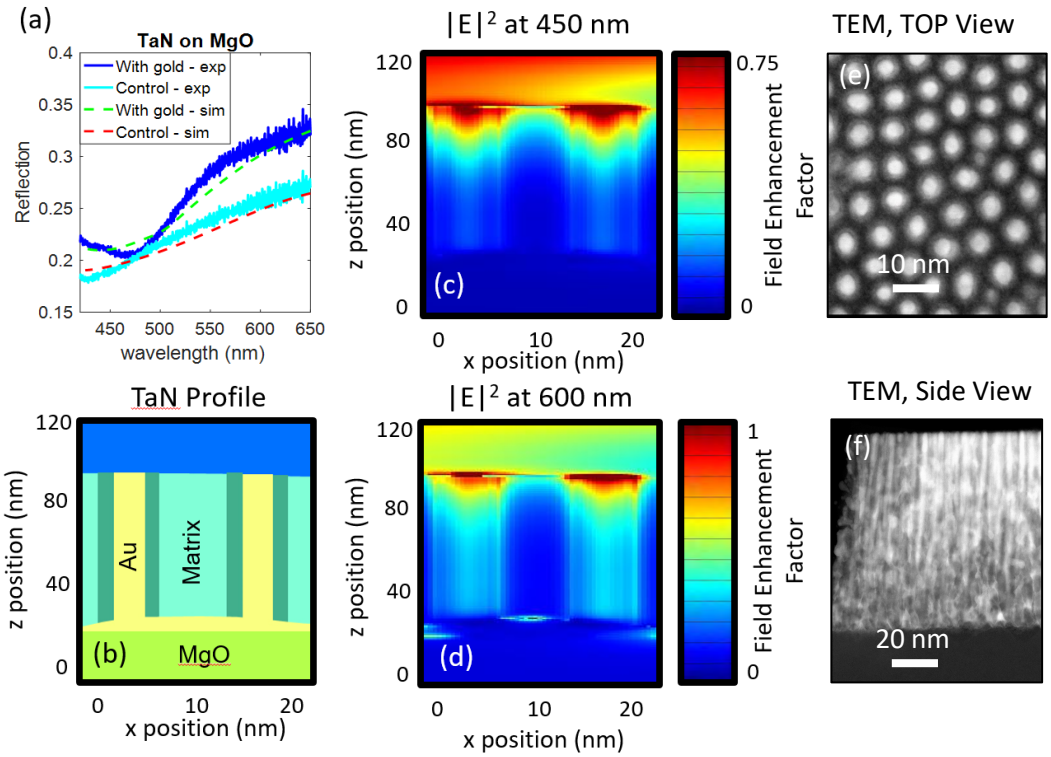

Figure 3 (a) Comparison of the experimental and simulated reflections of TaN with and without gold nano-pillars. (c) and (d) are the electric field enhancement at 450 and 600 nm respectively of the modeled geometry in (b) composed of gold pillars with a TaN cladding in a matrix of 20:80 TaN:Ta3N5 on MgO. (e) and (f) show the top view and side TEM of the wafer scale nanostructured film. The high absorption at normal incidence and pronounced anisotropy of the angle dependent thermal emission is expected to provide significantly greater temperature increases under solar illumination than can be achieved with more conventional lithographically define periodic metal nanostructures.

To reach the highest possible temperatures, very high angular anisotropy of the absorption is required. That is, as summarized above, there needs to be very high absorption at normal incidence, with little thermal emission at more oblique angles. In order to achieve this more rigorous optical constraint, it is necessary to define nanoscale order with very high aspect ratios of the resonant nanoscale features. In particular we predict that highly ordered arrays of plasmonic nanowires oriented normal to a film surface can achieve the highest possible temperatures in an all metal structure bases on periodic resonances. The basic electromagnetic design of this class of materials, sometimes termed ‘hyperbolic metamaterials’ due to the large anisotropy in the angle dependent permittivity, has recently been the subject of intense research activity in the nano-optics community.

While difficult to fabricate using conventional top-down lithographic fabrication procedures, we have initiated a fruitful collaboration with Prof. Haiyan Wang (Electrical Engineering, Purdue University), who has developed a procedure for co-sputtering metal with refractory insulators, in order to promote epitaxial growth of metal inclusion with a high degree of periodic order across macroscopic wafers, as well as unprecedented

aspect ratios and < 20 nm periodic spacing. Our initial collaborative work studying the optical behavior of the material platform was published in 2016, before YIP support. More recently, under the YIP program, we have published a manuscript **(3)** looking more in detail at the optical response (summarized in Figure 3), and we are working with Prof. Wang to develop a metal-cladding combination that is optimized for solar-induced temperature increases. Our role in the study has been to outline theoretical targets for fabrication, to provide the comprehensive spectral characterization and optical modeling, and eventually, to integrate films into test devices for optically-induced temperature determination and measurement of HEETE optical power conversion efficiency.

2) Electron Transport Across Asymmetric Plasmonic Junctions

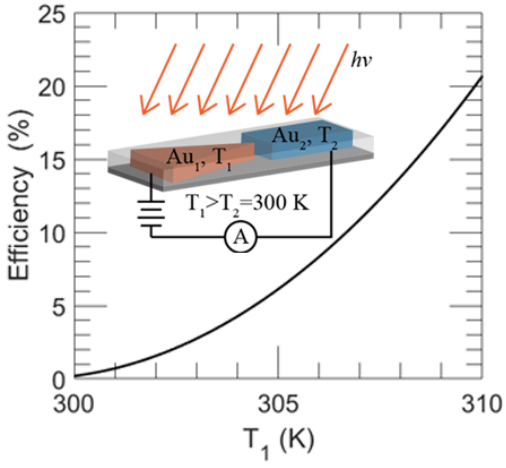

Figure 4 A schematic of a modeled tunneling device with a 1 nm tunnel gap. Enhanced optical absorption in the triangle-shaped electrode gives larger photothermal temperature increases and hot carrier generation for a tunneling current from the sharp tip to the rectangular electrode. The modeled conversion efficiency is plotted as a function of the temperature gradient across the junction under solar illumination.

We have performed an analysis of light-induced transport across tunnel junctions that can be employed for optical power conversion **(2)**. Optical and photochemical power converters based on resonant absorption in metal nanostructures generally employ a mechanism whereby optically excited 'hot' carriers are injected over a Schottky barrier at a semiconductor or molecular interface. This process is inefficient because most of the excited carriers relax and thermalize with the lattice before they can be collected. In contrast, we have outlined an alternative strategy that can take better advantage of both optically-excited and thermalized electrical carriers by leveraging tunneling transport phenomenon across metal junctions that concentrate and absorb light preferentially on one side of a nanoscale gap.

We have developed a general description for electron transport within a parabolic conduction band approximation accounting for both thermal (Fermi-Dirac) and non-thermal contributions to the steady-state electronic energy distribution that results from optical excitation. A non-zero current density is predicted when the excited-state distribution of carriers is dissimilar on opposite sides of a tunnel junction, with electrons emitted from the electrode that absorbs more light. An increase of the short circuit photocurrent and the associated open circuit voltage at elevated temperatures indicates a cooperative interaction between thermal and non-thermal excitation mechanisms. We also use full wave optical simulations (FDTD method) to demonstrate a simple device design for obtaining optical power conversion efficiency that is competitive with conventional photovoltaic (PV) devices.

In our study the role of photothermal heating and hot carrier excitation are analyzed separately, and our results indicate that both effects interact cooperatively to promote an electrical current from the electrode with greater local field concentration to the electrode with less field concentration. When only optically-induced thermal gradients

are considered, electron tunneling dominates transport across the junction both at room temperature and at elevated temperatures near 500 K. Photoexcitation of hot carriers under an optical flux comparable to solar illumination increases the current provided by the device, and allows for a theoretical optical power conversion efficiency of up to 80% when the junction is at an elevated temperature of 500 K and subject to a temperature gradient of 10K.Furthermore, full wave optical simulations of more realistic device geometries show that the directionality of the induced current flow is independent of excitation wavelength across the visible spectrum. Up to 20% power conversion efficiency is achieved in a modeled Au-TiO2-Au device structure under 707 nm monochromatic illumination with in intensity of 1000 W/m^2 when the junction is subject to a thermal gradient of ΔT = 10 K. We believe these results will inform strategies for more efficient device implementation of optical power converters based on plasmonic absorption in metals, specifically because we outline how “low grade” thermal excitations and low energy optical excitations of the electrons can still be utilized in a power cycle or for photochemistry.

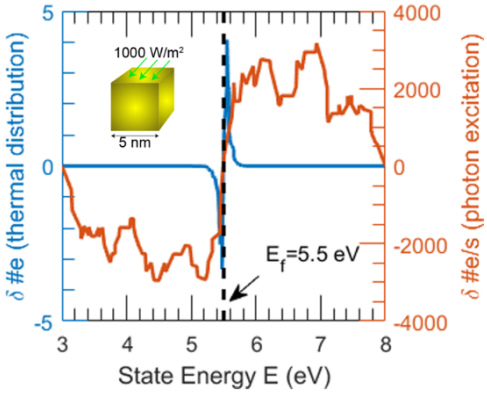

Figure 5 The hot electron generation rate under 532 nm monochromatic irradiation at a power density of 1000 W/m^2 compared with the thermal distribution of electrons in a 5 nm Au cube at 300 K.

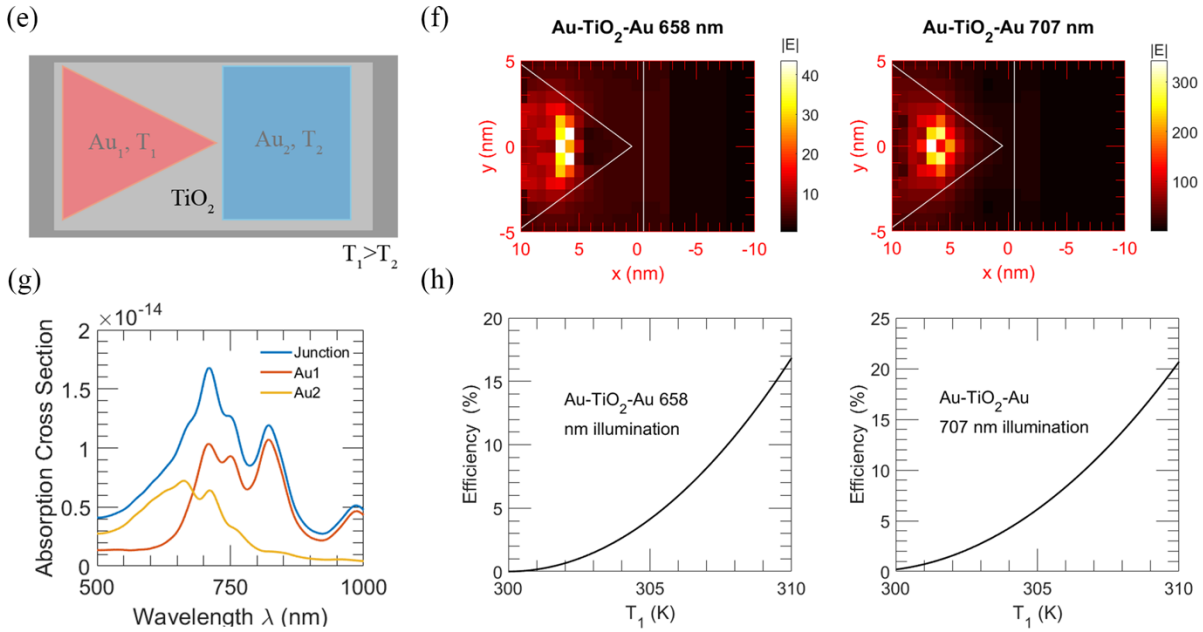

Figure 6 (e) Top-down schematic view of an Au-TiO2-Au device and (f) the corresponding electric field enhancement map of the 20 nm × 10 nm junction region for illumination at 658 nm (left) and 707 nm (right). (g) The calculated absorption spectrum (blue) of the device in (e) with the spatially-integrated absorption by electrode Au1 (red) and electrode Au2 (yellow). (h) Estimated conversion efficiency for 658 nm illumination (left) and 707 nm illumination (right). All calculations are for an optical power density of 1000 W/m2.

3) Electron Transport and Magnetism via Coherent Transfer of Photon Momentum

In addition to mechanisms for charge transport that result from photoexcitation and photo-thermalization, we have also studied conditions that promote the direct transfer of photon momentum to electron momentum in order to provide charge transport **(6)**. In particular, we have made significant progress understanding how circularly polarized radiation can induce circulating currents in metal nanostructures, giving rise to pronounced ultrafast optically-induced magnetism, and ultimately, new mechanism of photocurrent that we predict circulate the nanostructure, depending on the handedness of the incident radiation. The generation of magnetic fields by this mechanism is called the inverse Faraday effect (IFE), as outlined in Figure 7. In plasmonic systems the IFE can be mechanistically understood as resulting from the coherent solenoid-like circular electron motion in response to the circular polarized optical field (Fig. 7).

Strategies for ultrafast optical control of magnetism have been a topic of intense research for several decades because of the potential impact in technologies such as magnetic memory, spintronics, and quantum computation, as well as the opportunities for non-linear optical control and modulation in applications such as optical isolation and non-reciprocity. Recently we reported the first experimental quantification of optically induced magnetization in plasmonic Au nanoparticles due to the inverse Faraday effect (IFE). The induced magnetic moment is large under typical ultrafast pulse excitation ($<10^{14}$ W/m^2 peak intensity) and can easily exceed the magnetic moment in comparably sized magnetic nanoparticles such as magnetite by more than order of magnitude. Furthermore, the magnetization and demagnetization kinetics are instantaneous within the sub-picosecond time resolution of our studies, supporting a mechanism of coherent transfer of angular momentum from the optical field to the electron gas.

In order to measure induced magnetization in plasmonic nanoparticles produced by the IFE, we performed static and ultrafast pump-probe Faraday rotation measurements on 100 nm diameter Au nanoparticle colloids (AuNP). First, the spectrally-resolved Verdet constant was determined from static Faraday rotation measurements on the sample colloid solution in a 1 cm-pathlength cuvette. On the same sample in 2 mm-pathlength flowing cell (Fig. 8), the IFE was induced by a circularly polarized pump beam. The resultant magnetization was indicated by the Faraday rotation angle ($\Delta\theta$) of a linearly polarized probe beam. Based on the previously measured Verdet constant, the magnitude of the optical rotation of the probe thus enabled quantitative determination of the strength of the induced magnetization.

In order to further confirm a magnetic field was created during optical excitation, as opposed to other non-linear optical

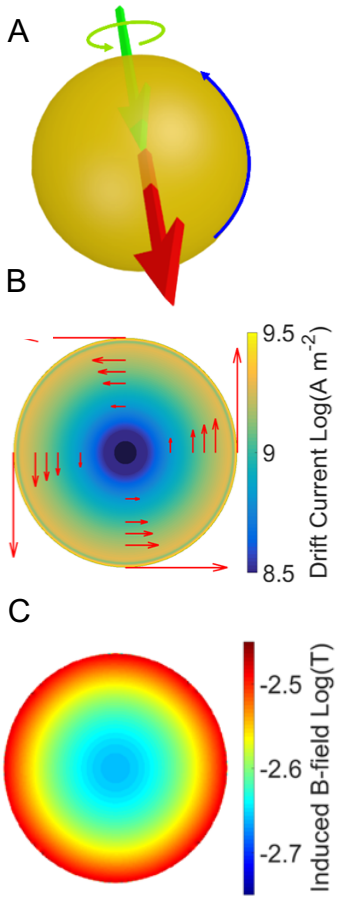

Figure 7 (a) Schematic of the Inverse Faraday Effect (IFE). Circularly polarized light (green) produces a static magnetic field (red) and circulating drift currents (blue) during illumination. (b) Calculated drift current and (c) magnetic field under 10^{12} W/m^2, in cross section, from our recent theoretical and computational study.

phenomena or photothermal heating that could contribute to the measured optical rotation, we also performed the IFE experiment with counter-propagating pump and probe beams. This result confirms that a transient change in refractive index of the material (OKE) or any other photothermal effects are reciprocal for either direction of the probe beam with respect to the pump beam. Importantly, in contrast, the IFE depends strongly on the propagation direction of the pump and probe beams, confirming the presence of the magnetization that gives rise to the nonreciprocal Faraday rotation of the probe beam.

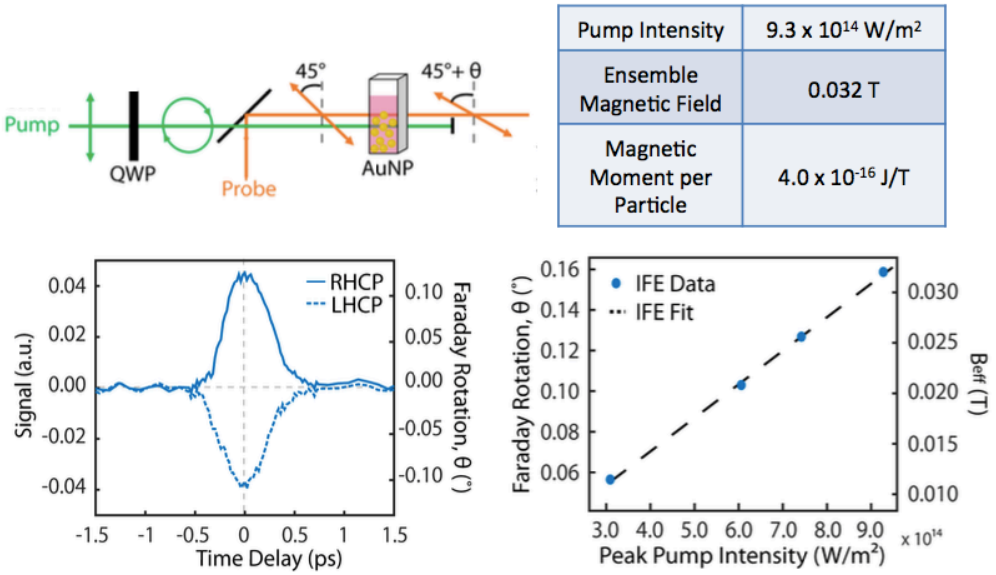

Figure 8 (top left) Schematic of our recently reported[1] experiment used to probe the IFE in 60 nm Au nanoparticle colloids. The induced magnetic field from a circularly polarized pump was indicated by the Faraday rotation of a linearly polarized probe beam. A pronounced optical rotation that switches sign based on pump chirality, corresponding to an equivalent applied external magnetic field of 32 mT was observed. The induced magnetic moment per particle of 4.0 x 10^{-16} J/T is approximately two orders of magnitude larger than the magnetic moment in other comparable magnetic nanoparticles such as magnetite or $CoFe_2O_4$ colloidal nanoparticles, and > 1000x stronger than reported for bulk Au.

4) Plasmonic Thermionic Devices for Optical Power Conversion

The most significant insights learned during our YIP supported studies are summarized in a recent report **(5)** in which we demonstrated that the proposed Hot Electron Enhanced Thermionic Emission (HEETE) mechanism can indeed open the door to new opportunities for highly efficient optical power conversion. Thermionic converters generate electricity from thermal energy in a power cycle based on vacuum emission of electrons. While thermodynamically efficient, practical implementations are limited by the extreme temperatures required for electron emission (> 1500 K). We have shown how metal nanostructures that support resonant plasmonic absorption enable an alternative strategy. High electronic temperatures required for efficient vacuum emission can be maintained during steady-state optical absorption while the lattice temperature remains within the range of thermal stability, below 600 K. We have also developed an optical thermometry technique based on anti-Stokes Raman spectroscopy (**Topic 5, below**) that confirms these unique electron dynamics. Thermionic devices constructed from plasmonic absorbers show performance that can out-compete other strategies of concentrated solar power conversion in terms of efficiency and thermal stability.

Top-down lithographic techniques were used to fabricate a 90 μm square array of 225 nm × 225 nm × 100 nm Au nanocubes at a pitch of 500 nm on a 150 nm thick gold film. The design was chosen to maximize optical absorption of 532 nm incident laser radiation, while also promoting strong field concentration at hot spots on the nanocubes where there is greater surface area intersecting escape cones for hot electron emission. Optical and SEM images are displayed in Fig. 9a, b. At the excitation wavelength (532 nm) there is an approximate 2-fold increase in absorption compared with a gold thin film (Fig. 1d), leading to increased photothermalization localized in the nanocubes.

In order to demonstrate that the hot electrons can perform work, we constructed a thermionic power convertor

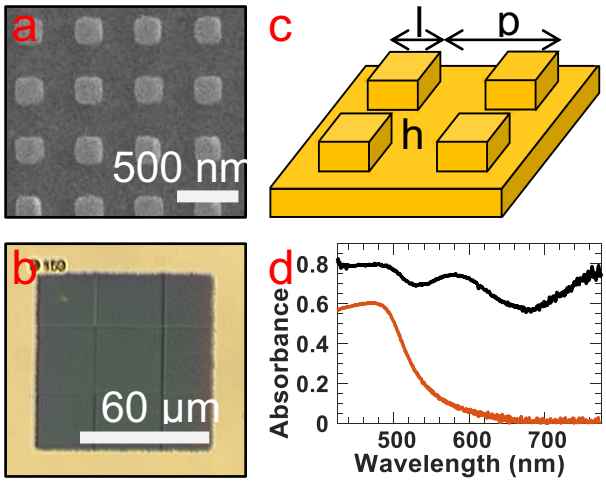

Figure 9 (a) SEM and (b) optical image of the fabricated nanostructure. The unit cell of the nanostructure is described by the schematic in (c) where l =225 nm, p = 500 nm, and h = 100 nm. (d) the absorbance of the nanostructure (black) compared to a smooth gold thin film with thickness = 150 nm (red).

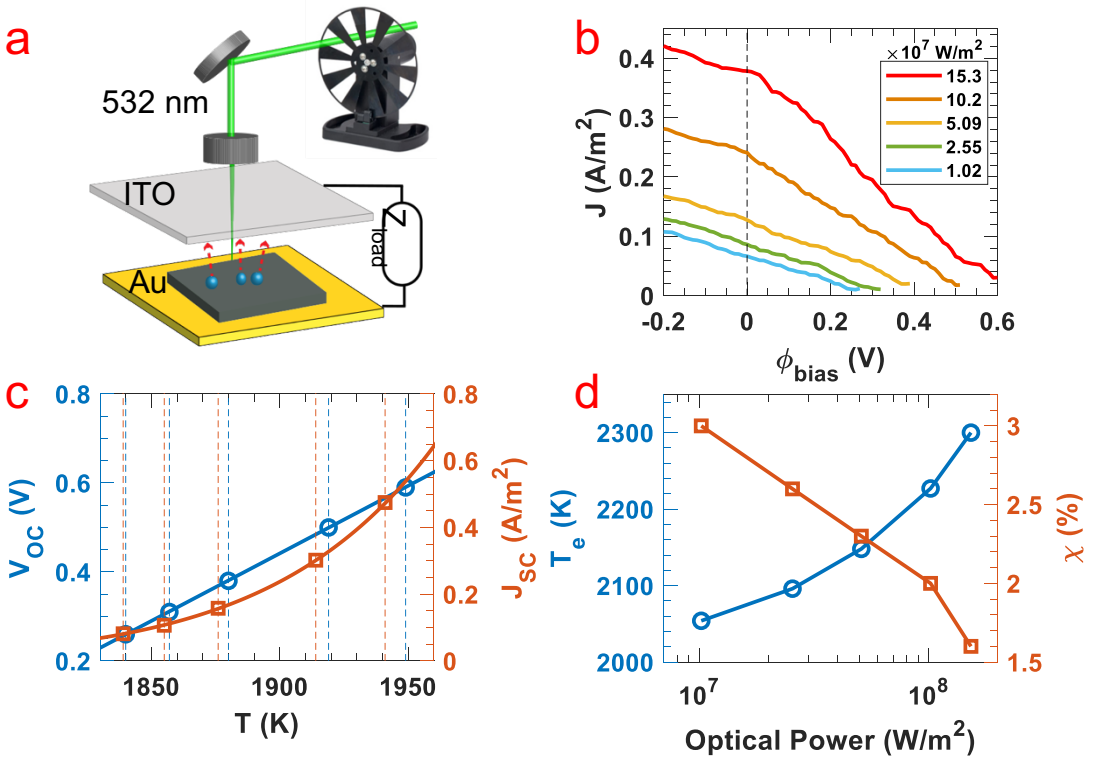

Figure 10 (a) Schematic of thermionic emission measurement. (b) J-V curve measured at different optical powers. (c) Measured J_{SC} (circle) and V_{OC} (square) versus the calculated temperature according to a one-temperature model. The vertical dashed lines indicate the discrepancies in calculated temperature based on J_{SC} (red) or V_{OC} (blue). (d) Fitted electronic temperature (circle) and percentage of hot electrons χ (square) according to a two-temperature model.

using the same nanostructure from Fig. 9 as an emitter with an ITO counter-electrode as a collector (Fig. 10a). The current density, J, was measured via a lock-in amplification scheme from parallel electrodes separated by 200 μm during 532 nm CW illumination under vacuum (0.010 mbar). The power generation region of the current-voltage (J-V) response is depicted in Fig. 10b. Since ITO contributes no signal in the experiment, the current density from the nanostructure asymptotically approaches zero as a retarding bias is increased. The open-circuit voltage (V_{OC}) reported here therefore represents the bias at which the current density reaches the noise level for the lock-in amplifier. The downward curvature of the J-V response indicates the presence of space charge effects during the measurement.

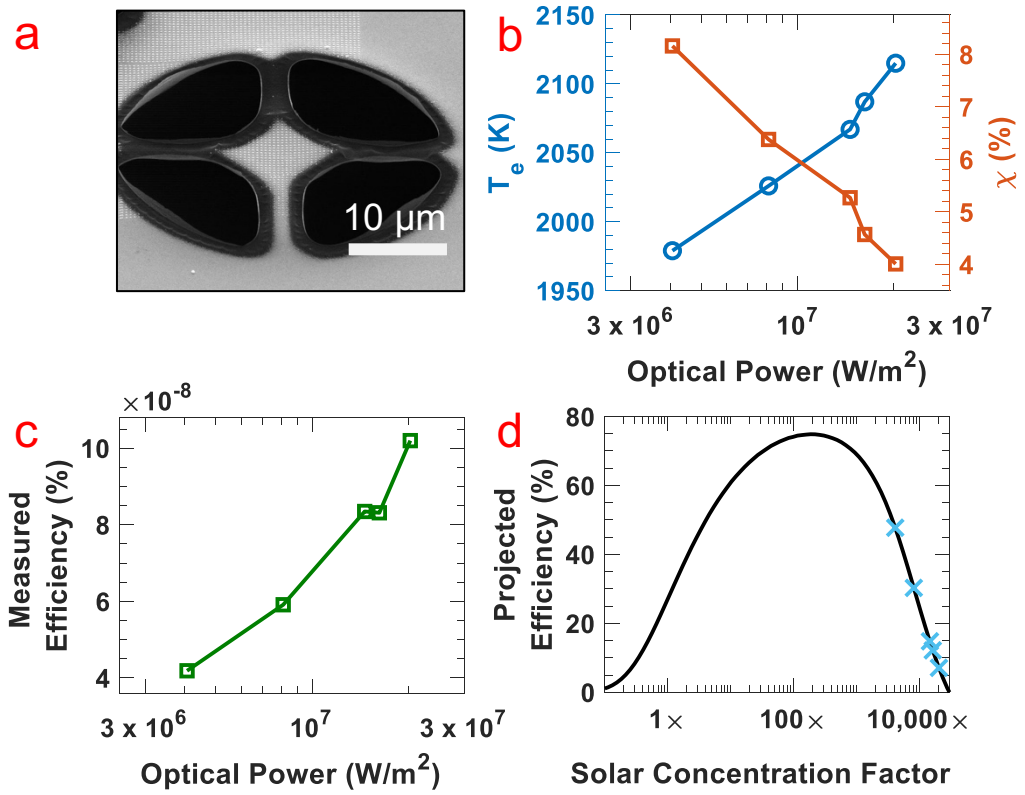

Figure 11 (a) SEM image of a thermally isolated gold nanostructure (b) Fitted electronic temperature (circles) and percentage of hot electrons (squares) according to a two-temperature model (c) Measured optical power conversion efficiency and (d) projected optical power conversion as a function of solar concentration factor, assuming a decreased work function, W = 1.6 eV. The blue crosses correspond to the optical powers measured experimentally.

To demonstrate the potential of this strategy for solar power conversion, an additional sample was prepared that minimized losses due to conduction. The nanostructure was fabricated on a 50 nm thick Si_3N_4 membrane. Focused ion beam etching was used to perforate the membrane and thermally isolate a 6 x 6 μm section of the array (Fig. 11). In vacuum, the device achieved optical power conversion efficiency between 10^{-8} –10^{-7} %, under 4×10^6 – 2.1×10^7 Wm^{-2}. This optical power range is comparable to that employed in solar-thermal conversion schemes, where solar concentration factors are commonly between 1500 – 4000x. While the sample showed no evidence of thermal degradation or melting, the seemingly low efficiency is due to the

large work function of gold, W = 5.1 eV. It is common practice during thermionic device operation to include rarified Cs metal vapor to both decrease W via surface adsorption and minimize space charge effects. Cesiated gold surfaces have a reported work function of W = 1.6 eV. Assuming the same photo-thermal response measured here but with W = 1.6 eV, a maximum conversion efficiency of 74.9% is predicted to occur at 190x solar concentration. If practically achievable, such high efficiency for collecting hot electrons would significantly decrease the optical energy that is available to promote heating of the lattice through electron-phonon coupling, further promoting stability of the emitter. For comparison, state-of-the-art solar-thermal conversion strategies achieve ~30% efficiency commonly at temperatures greater than 1000 K.

5) In-situ Anti-Stokes Raman Spectroscopy for Quantifying Hot Electrons

The same samples that were analyzed for optical power conversion performance were also studies spectroscopically using a new method of anti-stokes Raman thermometry that was developed in our lab for quantifying the steady-state population of photo-excited hot electrons, hot electron lifetime, lattice temperature, and electron-phonon coupling in plasmonic structures.

Temperature measurements during photothermalization were achieved by collecting anti-Stokes Raman spectra under 532 nm continuous wave (CW) laser illumination. A representative anti-Stokes spectrum is shown in Fig. 11. The signal from the nanostructure is ~10x larger compared to a gold thin film, comparable with enhancements often observed in surface enhanced Raman studies. Direct scattering from phonons does not contribute to the Raman signal from noble metal, therefore the broad frequency response is due to an anti-Stokes interaction directly with the electron gas. The physical origin of this anti-Stokes signal is still under some debate, with recent studies providing evidence that the signal may be due to photoluminescence rather than coherent scattering as in conventional Raman spectroscopy. Regardless of the microscopic mechanism, the spectral-dependent intensity of the anti-Stokes spectrum has been established as an accurate indicator of the lattice temperature of a noble metal. The signal intensity therefore follows the Bose-Einstein thermal distribution of lattice excitations, as in eq. 1.

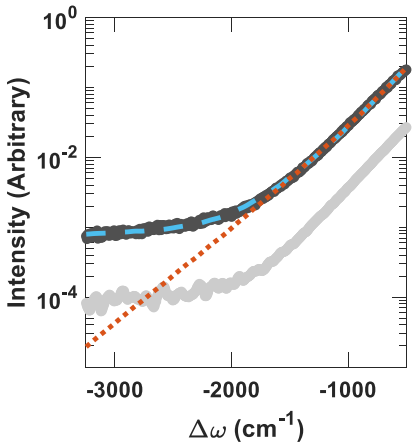

Figure 11 Measured anti-Stokes Raman signal from the nanostructure (solid black) and gold film (solid grey), both collected under 7.3 × 10^9 Wm^{-2} 532 nm laser excitation. The fit to a one-temperature model (eq. 1, red dotted) and two-temperature model (eq. 2, blue dash) are shown. The one-temperature fit gives T = 459 K, while the two-temperature fit gives T_l = 430 K, T_e = 10,040 K, and χ= 0.34%.

$$I(\Delta\omega) = C * D(\Delta\omega) * \left(\frac{1}{e^{\frac{hc\Delta\omega}{kT_l}} - 1} \right) \qquad (1)$$

Here, I is the anti-Stokes signal intensity normalized by power and integration time as a function of the energy difference, $\Delta\omega$, from the Rayleigh line in m^{-1}, and T_l is the lattice

temperature in K. This expression includes a constant scaling factor, C, to account for experimental collection efficiency that is re-calibrated for each measurement. In addition, the signal intensity is proportional to the density of optical states, $D(\Delta\omega)$, obtained from the reflection spectrum.

Fitting our data to eq. 1 (Fig. 11, red dash) proves inadequate as there is a large signal at high energy Raman shifts greater than -2000 cm^{-1} that is not well described by the Bose-Einstein distribution. However, our data is readily described if additional terms are included to account for a sub-population of hot electrons, χ, with an energy distribution at an elevated temperature, T_e.

$$I(\Delta\omega) = C * \chi * D(\Delta\omega) * \left(\frac{1-\chi}{e^{\frac{hc\Delta\omega}{kT_l}} - 1} + \frac{\chi}{e^{\frac{hc\Delta\omega}{kT_e}} + 1} \right) \qquad (2)$$

The magnitude of χ in the steady state depends on both the generation rate of hot electrons due to optical excitation, and the relaxation rate as they equilibrate to T_l via phonon scattering. Those carriers in thermal equilibrium with the lattice follow Bose-Einstein statistics, while the high-energy tail of the Raman signal is described by Fermi-Dirac statistics, as expected for a thermal distribution of hot electrons. The fit to this two-temperature model (TTM) in Fig. 11, (blue dash) is excellent for all samples and optical powers probed, spanning 10^7 to 10^{11} Wm^{-2}.

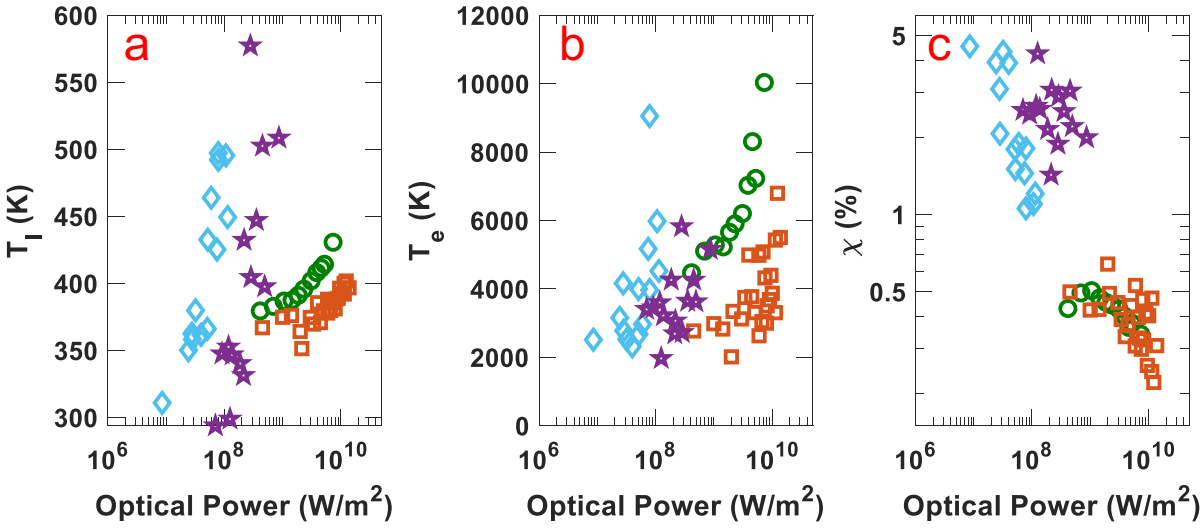

Figure 12 The TTM fit for (a) lattice temperature, (b) electronic temperature, and (c) the percentage of hot electrons. These data are for the nanostructure under vacuum (blue diamonds), nanostructure in atmosphere (green circles), a gold thin film under vacuum (purple stars), and a gold thin film in atmosphere (red squares)

The dependence of T_e, T_l, and χ on optical power for the optimized nanostructure and for a 150 nm thick gold thin film control was determined by analyzing the Raman spectra with respect to the TTM in eq. 2. Samples were measured at atmospheric pressure and under vacuum (0.010 mbar). The fitted data is summarized in Fig. 12. The lowest optical power studied was limited by the signal-to-noise ratio required to fit the TTM. There is a larger spread in the data for samples under vacuum due to a smaller

signal-to-noise ratio in that collection geometry. However, the enhanced Raman signal from the nanostructure allowed for studies at a significantly lower optical power range. Melting and degradation of the samples occurred when the fitted T_l significantly exceeded ~ 600 K in vacuum. In addition, the formation of a surface coating of gold oxide was apparent when T_l exceeded ~ 450 K for samples in atmosphere so data above those temperatures is omitted from this analysis.

In all experiments we observed a monotonic increase in T_e and T_l as the optical power increased, with T_e in excess of T_l by at least an order of magnitude. This trend is expected due to the lower heat capacity of the electron gas, and the values we measure for T_e and T_l are similar to those reported in transient absorption (TA) experiments. To date, TA experiments have been the primary method for probing electron dynamics in plasmonic nanostructures, however our experiments also access lower optical powers than can be achieved in pulsed time-resolved studies. Due to the decrease in convection, there is both a higher fitted T_e and T_l for samples under vacuum compared to samples in atmosphere. In addition, in all studies the nanostructure reaches significantly higher T_e and T_l than the gold thin film at equivalent optical power, due to the greater absorption and photothermalization provided by the plasmonic resonances.

A unique capability of our experiments that cannot be achieved readily in pulsed TA studies of electron dynamics is an analysis of the total size of the hot electron population, χ, during steady-state illumination. Thus, an analysis of χ from our fitted spectra provides important new information about how the availability of hot electrons depends on optical power and temperature under CW illumination that is more directly comparable to operating conditions for emerging hot-electron-based technologies. Interestingly in all experiments we observe a clear inverse correlation between T_e and χ as optical power increases. One may initially expect that increases in optical power would lead to a greater rate of electronic excitation and thus a larger steady-state population of hot electrons. We hypothesize the opposite behavior is due to the increase in electron-

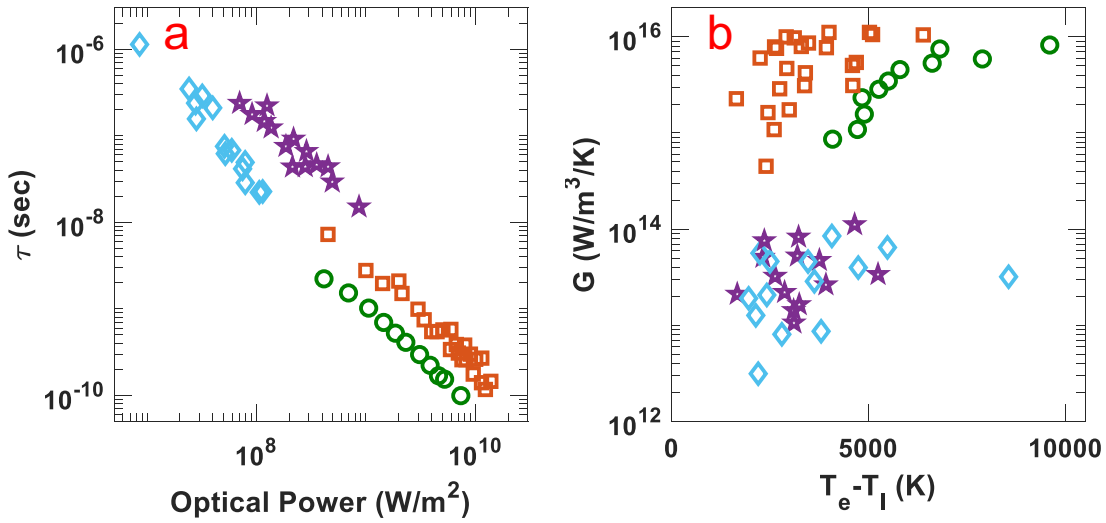

Figure 13 (a) Calculated lifetime and (b) coupling constant for the nanostructure under vacuum (blue diamonds), nanostructure in atmosphere (green circles), gold thin film under vacuum (purple stars), and a gold thin film in atmosphere (red squares).

phonon coupling as temperature increases, providing faster relaxation of the hot electrons that overwhelms the increase of the excitation rate. Our hypothesis is supported below by an analysis of the hot electron lifetime, τ, and electron-phonon coupling constant, G, both calculated from χ, also allowing for direct comparison of our findings with established TA measurements and computational studies.

The lifetime of hot electrons within the elevated temperature distribution can be determined by comparing the size of the steady-state sub-population of hot electrons with the rate of hot electron generation. If it is assumed that every absorbed photon produces a transiently excited electron, then

$$\tau = \frac{\chi \rho V}{N \sigma} \tag{3}$$

where ρ is the electron density of gold, V is the volume of the metal interacting with the light, N is the incident number of photons per second, and σ is the experimentally measured absorbance. As can be seen in Fig. 13, for all four data sets there is a monotonic decrease in τ as the incident optical power is increased. At the highest optical powers τ approaches picosecond timescales, in agreement with TA measurements at similar powers. Further, samples under vacuum show significantly longer τ than those at atmospheric pressure. We hypothesize that this difference may be due to surface collisions with gas molecules such as oxygen. The observation of Au-oxide formation at higher optical power provides further evidence that hot electrons interact with oxygen during illumination.

Further analysis of χ allows us to determine the electron-phonon coupling constant, G, independently from the lifetime. In the TTM well-established in TA studies, the time response of T_e is related to volumetric electronic heat capacity, C_e, by the following relation:

$$\chi \frac{\partial (C_e T_e)}{\partial t} = \chi G (T_e - T_l) + Q \tag{4}$$

Where G is the coupling constant in $Wm^{-3}K^{-1}$ and Q is the incident power in Wm^{-3} coupled into the absorbing volume of the metal. We solve for G, as the time derivative goes to zero in the steady state. We have shown above that at atmospheric pressure there are significant environmental contributions to the hot electron lifetime, implying that G accounts for coupling to all relaxation pathways. However in vacuum it is expected that electron-phonon coupling will dominate relaxation.

For all samples there is an increase in the G as a function of temperature, in agreement with *ab initio* calculations and experimental studies. Notably, in atmosphere the gold thin film exhibits a larger G than the nanostructure at the same optical power. In vacuum the environmental influences are minimized, and within the spread of the data, the nanostructure and thin film show an equivalent coupling constant that agrees with calculated values for nanoscale gold. We hypothesize this trend in G is due to a decrease in the active surface area with hot electrons, likely near electromagnetic hot spots, and that only gas molecule collisions in these locations contribute to relaxation. The net result is that the nanostructure achieves much greater T_e under equivalent optical power, and further, hot electrons have longer lifetimes compared with thin films at the same T_e in

atmosphere. Both behaviors are desirable in devices that take advantage of hot electrons, and our results suggest optical designs that decrease the relative volume in which hot electrons are generated could further optimize this response.

Summary: We have demonstrated a variety of new opto-electronic power conversion mechanisms that uses plasmonic nanostructures to promote electron emission and transport for optical power conversion and photochemistry. Our work has culminated in a strategy that allows for decoupled electronic temperature and lattice temperature during steady-state optical illumination of a thermionic emitter. We have also developed an optical thermometry technique based on anti-Stokes Raman spectroscopy to quantify these separate temperatures, as well as the size of the sub-population of hot electrons. Our results show an inverse relationship between the temperature and the population of the hot electron gas, and analysis of the lifetime and electron-phonon coupling show how designs that decrease the volume of the metal can further optimize the hot electron dynamics. When integrated into thermionic devices the plasmonic cathodes provide optical power conversion efficiency consistent with the electronic temperature, while maintaining significantly lower lattice temperatures. Thus, we demonstrated how this HEETE mechanism can overcome challenges related to thermal stability that have historically limited the use of thermionic devices for solar-thermal energy conversion. We believe the remarkable tailorability of plasmonic nanostructures may allow further opportunities for very efficient solar energy conversion based on this strategy.

Grant-Supported Publications:

1) B. Roman, M. Sheldon, "Six-fold Plasmonic Enhancement of Thermal Scavenging via $CsPbBr_3$ Anti-Stokes Photoluminescence", *Nanophotonics*, 2019, 8, 599-605. DOI: https://doi.org/10.1515/nanoph-2018-0196

2) S. Wu, M. Sheldon, "Optical Power Conversion via Tunneling of Plasmonic Hot Carriers", *ACS Photonics* 2018, 5, 6, 2516-2523, DOI: https://pubs.acs.org/doi/abs/10.1021/acsphotonics.8b00347

3) M. Sheldon (12 out of 13), H. Wang, "Nanoscale Artificial Plasmonic Lattices in Self-Assembled Vertically Aligned Nitride-Metal Hybrid Metamaterials", *Advanced Science* 2018, 5, 1800416, DOI: https://doi.org/10.1002/advs.201800416

4) A. Pravitasari, M. Negrito, K. Light, W. Chang, S. Link, M. Sheldon, J. Batteas, "Using Particle Lithography to Tailor the Architecture of Au Nanoparticle Plasmonic Nanoring Arrays" *The Journal of Physical Chemistry B* 2017, 122(2), 730–736. DOI: https://pubs.acs.org/doi/10.1021/acs.jpcb.7b06357

Submitted for Publication:

5) S. Wu, N. Hogan, M. Sheldon, "Hot Electron Dynamics in Plasmonic Thermionic Emitters" submitted to *Nature Nanotechnology* 2019, see arXiv: http://arxiv.org/abs/1905.01580

6) O. H. Cheng, D. H. Son, M. Sheldon, "1,000-Fold Enhancement of Light-Induced Magnetism in Plasmonic Au Nanoparticles", *Nature Photonics* 2019 (*requested revisions submitted*) see arXiv: https://arxiv.org/abs/1904.11425

In Preparation:

7) (Invited Feature Article for *Journal of Physical Chemistry*) S. Wu, N. Hogan, M. Sheldon, "Mechanisms of Electrochemical Potential During Plasmonic Absorption"